DETERMINATION OF PHYSICAL PROPERTY PARAMETERS OF CLAYEY SOIL IN RICE STRAW FIELDS AND CALIBRATION OF DISCRETE ELEMENT SIMULATION PARAMETERS

/

稻茬田黏重土壤物性参数测定与离散元仿真参数标定

Jixuan WANG[1,2], Lan JIANG[1,4], Qing TANG[1,2,3,4], Subo TIAN[2], Jing LUO[1], Jun WU[1,4], Zhuohuai GUAN[1,4], Yaodong WU[3], Qun LI[3], Meng BAI[1]

[1] Nanjing Institute of Agricultural Mechanization, Ministry of Agriculture and Rural Affairs, Nanjing 210014, China;
[2] Shenyang Agricultural University, Shenyang 110866, China;
[3] Jiangsu Yunma Agricultural Machinery Manufacturing Co., Ltd., Yancheng 224100, China
[4] Key Laboratory of Modern Agricultural Equipment, Ministry of Agriculture and Rural Affairs，Nanjing 210014, China
Corresponding author: Qing TANG
Tel: +86.15366092914; E-mail: tangqing01@caas.cn
DOI: https://doi.org/10.35633/inmateh-78-70

Keywords: *Heavy clay soil, Discrete element method, Parameter calibration, Soil penetration, Soil stiffness*

ABSTRACT

Soils in China's Yangtze River Basin are heavy and cohesive. During simulation studies of rotary tillage preparation, obtaining accurate soil fragmentation patterns has been challenging due to the lack of precise soil discrete element parameters. This study calibrated the physical and contact parameters of heavy clay soils using the EDEM discrete element method. Soil density, shear modulus, Poisson's ratio, collision recovery coefficient, static friction coefficient, and rolling friction coefficient between soil-soil and soil-tiller components were experimentally determined. Soil penetration tests were conducted using the Hertz-Mindlin with JKR contact model in EDEM software. A Plackett-Burman design identified four parameters significantly influencing soil penetration stiffness: soil-soil collision recovery coefficient, soil-soil static friction coefficient, JKR surface energy, and soil-soil rolling friction coefficient. Building upon this, a second-order regression model linking soil firmness to key parameters was established via Box-Behnken experiments. An optimization algorithm was then employed to determine optimal parameter values, yielding the following combination: soil-soil static friction coefficient 0.441, soil-soil collision recovery coefficient 0.537, and JKR surface energy 9.551 J/m². Validation results demonstrated that under optimal parameters, the simulation error of soil stiffness compared to experimental data was only 3.0%, confirming the accuracy of the calibrated parameters.

摘要

中国长江流域土壤黏重，在旋耕整地仿真研究时，由于缺乏准确的土壤离散元参数，难以得到准确的土壤破碎规律。本研究基于 EDEM 离散元法对黏重土壤的物理与接触参数进行标定。试验测定土壤密度、剪切模量、泊松比以及土壤-土壤、土壤-触土部件间的碰撞恢复系数、静摩擦因数和滚动摩擦系数，采用 EDEM 软件中 Hertz-Mindlin with JKR 接触模型对土壤进行穿刺试验。采用 Plackett-Burman 试验筛选出对土壤穿刺试验坚实度影响显著的四个参数：土壤-土壤碰撞恢复系数、土壤-土壤静摩擦因数、JKR 表面能及土壤-土壤滚动摩擦系数。在此基础上，通过 Box-Behnken 试验建立了土壤坚实度与关键参数间的二阶回归模型，并采用优化算法进行参数寻优，最终获得最优参数组合：土壤-土壤静摩擦因数 0.441，土壤-土壤碰撞恢复系数 0.537，JKR 表面能 9.551 J/m²。验证结果表明，在最优参数条件下，土壤坚实度的仿真结果与试验结果误差仅为 3.0%，证明了参数标定的准确性。

INTRODUCTION

China's agricultural soils exhibit diverse types, necessitating the determination of numerous soil parameters during discrete element simulation modeling. The accuracy of these parameters is a critical prerequisite for ensuring the reliability of simulation results. However, some researchers face limitations in measurement equipment, making it difficult to accurately obtain soil parameters. Therefore, establishing scientifically sound methods for soil parameter measurement and calibration holds significant importance (*Pang et al.*, *2023*).

Currently, research on parameter calibration for soil discrete element modeling both domestically and internationally has primarily focused on weakly cohesive soil types, such as sandy soils, dry soils, or rock. *Ucgul M et al. (2014)* calibrated simulation parameters for cohesive and non-cohesive soils by combining angle-of- repose tests with the Hertz-Mindlin and Hysteretic Spring contact models, addressing issues such as plastic deformation under loading. *Aikins et al.* (*2021*) calibrated contact parameters for the Hysteretic Spring and Linear Cohesion models in cohesive soils using soil angle of repose tests. *Xinliang Tian et al.* (*2021*) established a discrete element model for corn stover-soil mixtures by determining the angle of repose of the mixture as a calibration indicator using the cylinder lift method, and systematically optimized the model's key micro-parameters. *Jingbin Sun et al. (2022)* focused on sloping clay loam soils, calibrating inter-particle contact parameters using a simulated angle-of- repose optimization method. *Long Zhou et al. (2022)* precisely calibrated discrete element contact parameters for soil-seed mixtures using the cylinder lift method and soil surface slope slip tests, providing theoretical basis for optimizing precision seeding equipment design. *He et al.* (*2024*) calibrated saline-alkali soil using the Hertz-Mindlin with Johnson-Kendall-Roberts contact model, with the angle of repose as the evaluation indicator. *Peishi Zou et al.* (*2025*) employed angle of repose tests to identify key discrete element parameters influencing the tillage process of white-slime soils. However, for highly cohesive soil types such as heavy clay soils and paddy soils, the angle of repose fails to accurately reflect their soil conditions. On one hand, the strong cohesive and adhesive forces between clay particles make it difficult for traditional contact models to accurately characterize their mechanical behavior. On the other hand, changes in moisture content significantly affect the mechanical properties of clay soils, increasing the complexity of parameter calibration. Therefore, conducting parameter calibration studies for cohesive soils and establishing contact models and calibration methods suitable for highly cohesive soils (*Mi et al., 2025*) has become a critical issue requiring urgent resolution in the field of soil discrete element simulation.

Xifeng Liang et al. (*2024*) through piston extraction tests, the discrete element contact model for tidal flat soil was optimized, enabling effective simulation of tidal flat soil properties. This holds significant importance for simulating the operating conditions and optimizing the design of tidal flat working equipment. *Bahrami et al.* (*2020*) through discrete element method (DEM) simulations of plate settlement tests, the influence patterns of key micro-parameters—such as cohesion and elastic collision recovery coefficient—on soil settlement characteristics were revealed. *Jin Zhang et al.* (*2021*) using the angle of repose test (cylinder lift method) and soil firmness test (penetration resistance) as dual response indicators, the cohesive parameters between soil particles and the interface characteristics between soil and agricultural machinery components were calibrated. These studies provide crucial parameter references and methodological guidance for discrete element simulations under varying soil conditions. Soil penetration tests focus on “resistance to failure under localized loading” suitable for analyzing soil bearing capacity and dynamic response, applicable to both cohesive and non-cohesive soils. Angle of repose tests focus on “natural accumulation characteristics under unconstrained conditions” primarily reflecting the flowability and looseness of non-cohesive soils. Both tests are utilized in discrete element parameter calibration. However, the penetration test is more sensitive to parameters like cohesion (suitable for cohesive soils), while the angle of repose test is more sensitive to friction coefficients and particle shape (suitable for non-cohesive soils). Therefore, employing the soil penetration test method in this study yields greater accuracy.

This study addresses the issue of unclear parameters in discrete element models for heavy clay soils (*Adajar et al.*, *2021*) Using soil samples from Southeast Village, Xixiaju Town, Xinbei District, Changzhou City, Jiangsu Province, the research employs the “Hertz-Mindlin with JKR” contact model within EDEM software. Through comparative soil penetration simulation experiments, the study systematically achieves precise calibration of parameters for the heavy clay soil discrete element model. This research aims to provide a reliable parameter foundation and simulation basis for subsequent in-depth investigations into the interaction mechanism between heavy clay soils and soil-contact components.

MATERIALS AND METHODS

Soil sampling

On December 12, 2024, at Southeast Village, Xixiaju Town, Xinbei District, Changzhou City, Jiangsu Province (31.93°N, 119.83°E), soil samples were collected using a soil sampler with the five-point sampling method (*Smith W. et al , 2013)*.

Soil density

Soil density was determined using the volumetric displacement method. A known mass of oven-dried soil was placed in a container, which was then filled with water. The water filled the void spaces within the soil, allowing the sample volume to be determined by displacement. The mass and volume of the added water were calculated using Equations (1) and (2).

$$M_b = M_z - M_t \quad (1)$$

$$V_s = \frac{M_b}{\rho_s} \quad (2)$$

where: M_b is the mass of the added water, [g]; M_z is the total mass of soil and water, [g]; M_t is the mass of the dry soil, [g]; V_s is the volume of the added water, [cm³]; ρ_s is the density of water, [g/cm³].

The soil volume and particle density were then calculated as:

$$V_t = V_c - V_s \quad (3)$$

$$\rho_t = \frac{M_t}{v_t} \quad (4)$$

where: V_t is the soil volume, [cm³]; V_c is the container volume, [cm³]; ρ_t is the particle density of the soil, [g/cm³]. The measured particle density of the soil was 2.655 g/cm³.

Soil moisture content

The soil moisture content was measured using a DHS-110-1 moisture tester (accuracy ±0.5%). The experiment was repeated five times, and the average soil moisture content was determined to be 23.48%.

Soil particle size distribution

A 1 kg oven-dried soil sample was subjected to sieve analysis using five standard sieves with aperture sizes of 3 mm, 2 mm, 1 mm, 0.5 mm, and 0.25 mm. The sieves were mechanically vibrated for 10 minutes to ensure uniform separation. After sieving, the mass of soil retained on each sieve was measured. Each test was repeated five times, and the results were recorded with an accuracy of 0.1 g. The sieved soil fractions are shown in Fig. 1, and the particle size distribution obtained from the sieve analysis is presented in Table 1. The results indicate that a high proportion of particles are smaller than 0.25 mm, suggesting that the soil is predominantly fine-grained.

Fig. 1 - Sieved soil particles

Table 1

Soil particle size distribution

Number	Particle size [mm]	Mass fraction [%]
1	0~0.25	50.15
2	0.25~0.5	12.59
3	0.5~1	22.39
4	1~2	8.74
5	2~3	5.16
6	≥3	0.97

Soil Poisson's ratio

Poisson's ratio of soil is defined as the ratio of lateral strain to axial strain under loading *(Tian et al., 2024)*. It can be determined through shear testing using a direct shear apparatus. During the test, several levels of normal stress were applied to the soil specimen, and the corresponding shear responses were recorded.

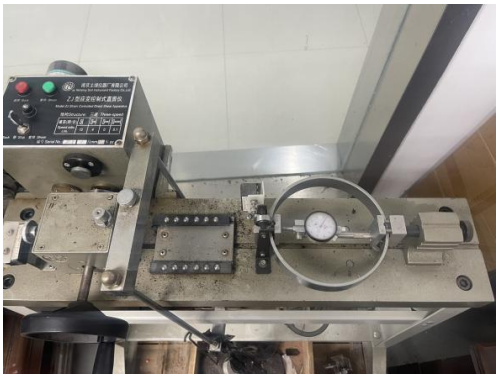

Fig. 2 - Soil Direct Shear Apparatus

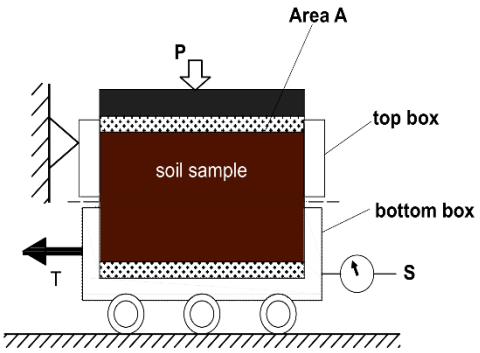

Fig. 3 - Schematic Diagram of the Direct Shear Test for Soils

By plotting the relationship between shear strength and vertical pressure, the soil's internal friction angle (φ) was determined to be 22.79°. Using equations (5) and (6), the soil's Poisson's ratio was calculated to be 0.38. This study used the classic Rankine approximate formula to correlate the internal friction angle (φ) with Poisson's ratio (v), which is a theoretical approximation rather than a result from direct experiments on the soil in the study area.

$$K = 1 - sin\varphi \tag{5}$$

$$v = \frac{K}{1 + K} \tag{6}$$

where: K is the soil pressure coefficient; φ is the soil's internal friction angle, [°]; v is the soil's Poisson's ratio.

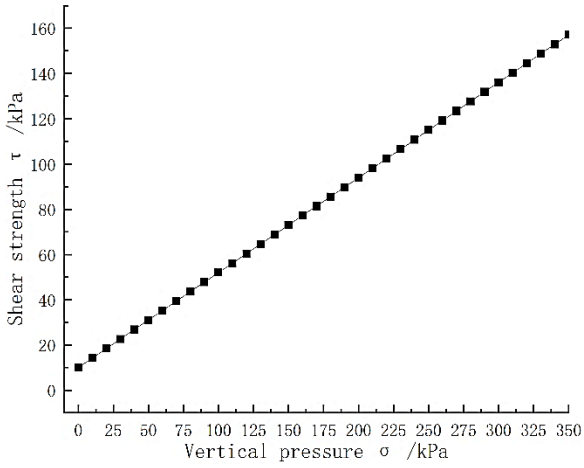

Fig. 4 - Shear Strength vs. Vertical Pressure Relationship Curve Diagram

Elastic modulus and shear modulus of soil

Standard cylindrical soil samples (diameter D = 50 mm, height L = 50 mm) were tested using a Shandong Zhongyi WDW-10 universal testing machine. Axial load was applied at a constant rate of 1 mm/s, and data on load (F) versus axial strain (ΔL) were collected (Figure 5).

Testing continued until the soil sample entered the plastic deformation stage and exhibited the descending segment of the stress-strain curve. Five replicate tests were conducted. The elastic modulus was calculated using Equations (7)-(9), and the shear modulus was determined via Equation (10).

$$\varepsilon = \frac{\Delta L}{L} \tag{7}$$

$$A = \pi\left(\frac{D}{2}\right)^2 \tag{8}$$

$$E = \frac{F}{A \times \varepsilon} \tag{9}$$

$$G = \frac{E}{2 \times (1 + v)} \tag{10}$$

where: ε is axial strain; ΔL is the deformation of the soil sample under compression, [m]; L is the original height of the soil sample, [m]; D is the diameter of the soil sample, [m]; A is the contact area of the soil sample, [m²]; F is the axial load applied to the soil sample, [N]; E is the elastic modulus, [Pa]; G is the shear modulus, [Pa]; v is Poisson's ratio.

Fig. 5 – Crushing test of soil sample

Collision recovery coefficient

The coefficient of restitution for soil-soil and soil-steel interactions was determined using the free-fall method. This parameter characterizes the ability of a material to recover after impact and reflects the energy dissipation during collision processes *(Diao et al., 2024)*. The experimental setup is shown in Fig. 6. A preformed soil block was released from a vertical height of 150 mm above the impact surface (soil plate or steel plate), resulting in a normal collision. After impact, the soil block rebounded and subsequently fell onto a receiving plate along an oblique trajectory. A high-speed camera was used to record the entire process, capturing the motion before and after impact. The rebound height was determined from the recorded images, allowing quantitative evaluation of the restitution characteristics at the contact interface. This method provides fundamental data for analyzing the impact behavior between soil and metallic materials.

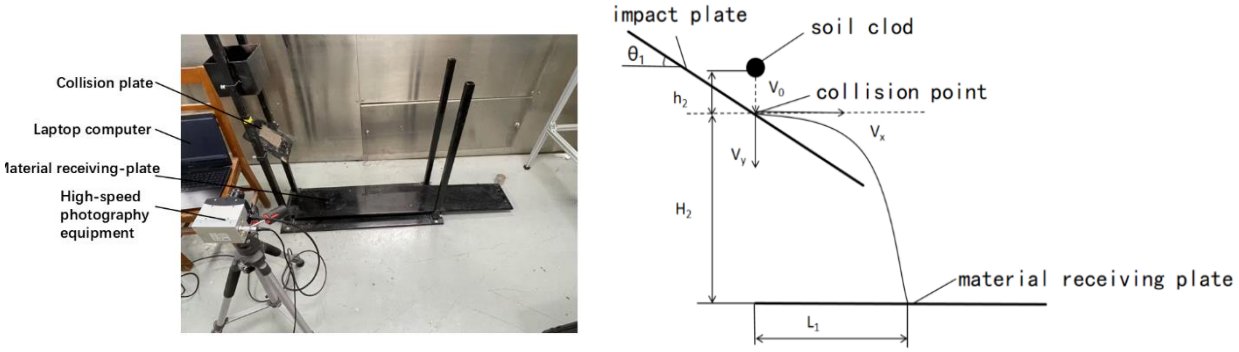

(a) *(b)*

Fig. 6 - Crash recovery coefficient measurement test

(a) Coefficient of Restitution Test Bench; (b) Measurement Principle of Coefficient of Restitution

The collision recovery coefficient was calculated using the following formula:

$$C_r = \frac{v_n}{v_n'} \tag{11}$$

$$v_n = v_1 \cos\left(\frac{\pi}{2} - \theta_1 + \arctan\frac{v_y}{v_x}\right) \tag{12}$$

$$v_n' = v_0 \sin\left(\frac{\pi}{2} - \theta_1\right) \tag{13}$$

$$v_1 = \sqrt{v_x^2 + v_y^2} \tag{14}$$

$$v_0 = \sqrt{2gh_1} \tag{15}$$

After the soil block collided with the impact plate, it underwent projectile motion, which is described by:

$$H_1 = v_y t + \frac{1}{2} g t^2 \tag{16}$$

$$L_1 = v_x t \tag{17}$$

where: C_r is collision recovery coefficient; v_n is normal velocity of soil block relative to impact plate prior to collision, [m/s]; v_n' is normal velocity of soil block after collision with impact plate, [m/s]; v_0 is velocity of the soil block upon reaching the collision point, [m/s]; h_1 is initial vertical distance between soil block and impact plate, [mm]; H_1 is vertical distance between soil block impact point and receiving plate, [mm]; L_1 is horizontal distance between soil block impact point and receiving plate landing point, [mm].

After repeating the test five times, the collision recovery coefficient between soil and soil was found to range from 0.20 to 0.70, while the collision recovery coefficient between soil and steel ranged from 0.05 to 0.55.

Static friction coefficient

The static friction coefficient between soil-soil and soil-steel interfaces was determined using the inclined plane method. As shown in Figure 7, the experimental setup consisted of an adjustable inclined plane platform and an angle measurement system.

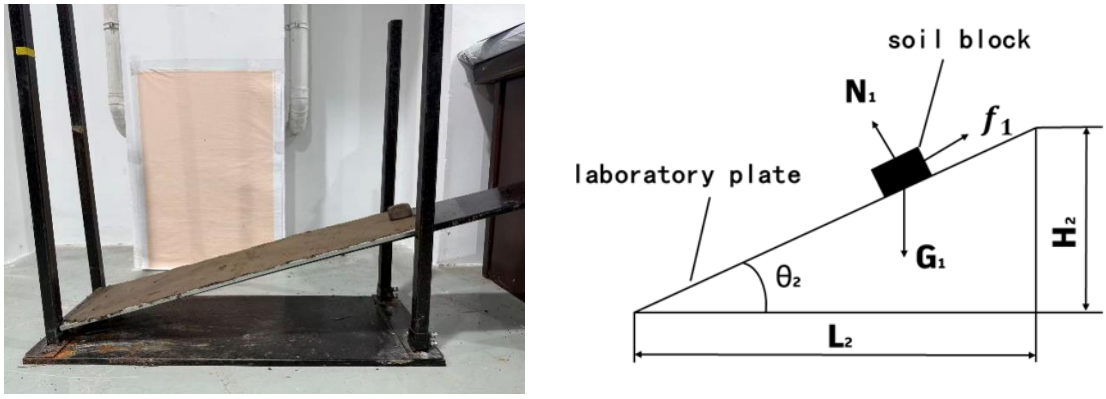

(a) (b)

Fig. 7 - Static friction coefficient measurement test

(a) Static Friction Coefficient Test Bench;(b) Measurement Principle of Static Friction Coefficient

When determining the coefficient of static friction between soil and a steel plate, the prepared and sieved soil was first evenly spread on the test plate and moistened thoroughly. After leveling, the soil layer was allowed to consolidate and air-dry for subsequent use. Meanwhile, the steel plate was fixed onto the inclined plane. During testing, the soil plate and steel plate were initially positioned horizontally. A soil sample was placed at the upper end of the contact surface. The inclined plane was then raised at a constant rate until the soil sample began to slide. At that moment, the adjustment was stopped, and the critical inclination angle was recorded. The coefficient of static friction was calculated based on this angle. Each test was repeated ten times, and the average value was taken to ensure reliability. The coefficient of static friction was calculated using:

$$\mu_1 = \frac{f_1}{N_1} = \frac{G_1 \sin\theta_2}{G_1 \cos\theta_2} = \tan\theta_2 \tag{18}$$

where: f_1 is sliding friction force, [N]; N_1 is plate support force on soil block, [N]; G_1 is soil block weight, [N]; θ_2 is instantaneous tilt angle of the plate when the soil block begins to move, [°].

Through repeated experimental measurements, calculations based on Equation (16) yielded the following results: the static friction coefficient between soil and soil ranged from 0.3 to 0.8, while the static friction coefficient between soil and steel ranged from 0.35 to 0.65.

Coefficient of rolling friction

The rolling friction coefficient between soil and steel plate was measured using the apparatus shown in Figure 8. Prepared soil balls were placed on a test plate inclined at an angle θ_3 to the horizontal plate and allowed to roll freely. The rolling distance on the horizontal plate was measured, and the test was repeated 10 times to calculate the rolling friction coefficient (*Diao et al.*, *2024*).

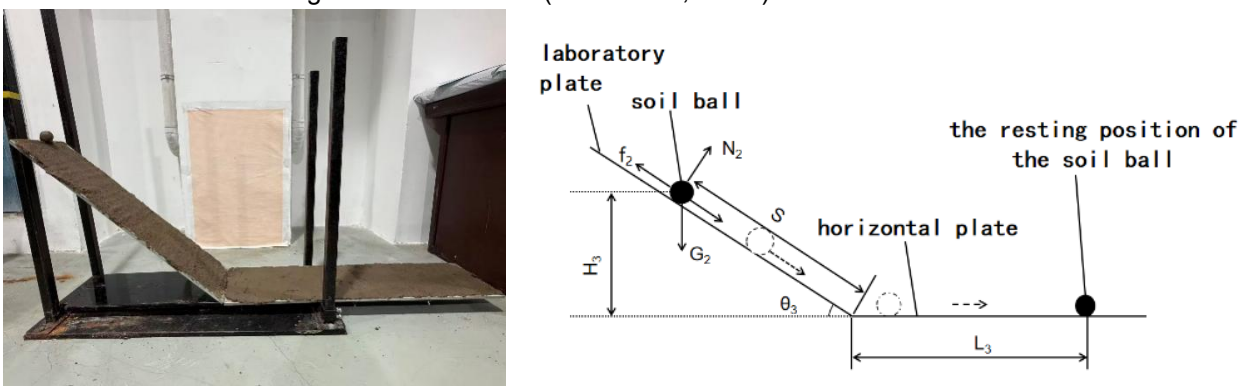

(a) *(b)*

Fig. 8 - Rolling friction coefficient measurement test

(a) Rolling Friction Coefficient Test Bench; (b) Measurement Principle of Rolling Friction Coefficient

According to the law of conservation of energy, the formula for calculating the rolling friction coefficient μ_2 is:

$$G_2 H_3 = \mu_2 G_2 (G_2 \cos\theta_3 + L_3) \quad (19)$$

where: G_2 is soil ball weight, [N]; H_3 is vertical distance between soil ball and horizontal plate, [N]; θ_3 is angle between test plate and horizontal plate, [°]; L_3 is soil ball rolling distance on horizontal plate, [mm].

Through repeated experimental measurements, calculations based on Equation (19) yielded the following results: the rolling friction coefficient between soil particles ranges from 0.1 to 0.6, while the rolling friction coefficient between soil and steel ranged from 0.05 to 0.25.

Soil puncture test

The soil penetration test is illustrated in Fig. 9 and was conducted using a universal testing machine, a standard soil penetrometer probe (30° cone angle, 12.83 mm base diameter), and a cylindrical container (80 mm diameter, 400 mm height). The collected soil was placed into the container without compaction. The probe was driven into the soil at a constant speed of 20 mm/s to a penetration depth of 50 mm. The force acting on the probe was recorded and transmitted to a computer for data acquisition. Each test was repeated five times using fresh soil samples. The peak penetration resistance was recorded for each test, and the average value was calculated as the soil firmness, which was 82.2 kPa.

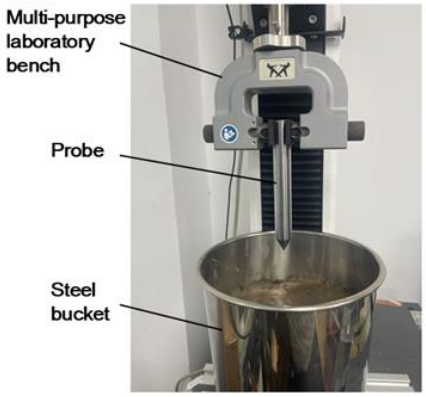

Fig. 9 - Soil Penetration Test

Soil contact parameter simulation calibration

First, the Plackett-Burman design was employed to screen key influencing factors. Second, the steepest ascent test was used to determine the optimization direction for each factor; finally, the Box-Behnken response surface method was adopted to establish a quantitative relationship model between factors and target values. The study targeted measured soil firmness as the objective value. Through analysis of variance and significance testing, three key factors significantly influencing soil firmness were identified. A factor-objective regression equation was established, ultimately determining the optimal parameter combination for the soil discrete element model.

Establishment of soil particle models

In this study, soil particles were generated based on the measured particle size distribution and corresponding mass fractions. Particles were assigned within each size interval to achieve a representative distribution consistent with the actual soil. When defining the particle generation parameters, the median value of each size interval was used as the particle radius, ensuring that the simulated particle size distribution approximated the real soil characteristics. To balance computational efficiency and simulation accuracy, the particle size in the simulation was scaled to five times the average particle size of the actual soil. The corresponding mass fraction distribution is presented in Table 2.

Table 2

EDEM soil simulation particle diameter and mass fraction

Particle size [mm]	Simulated particle diameter [mm]	Mass fraction [%]
0~0.25	0.625	50.15
0.25~0.5	1.875	12.59
0.5~1	3.250	22.39
1~2	7.500	8.74
2~3	12.500	5.16
3≤	15.000	0.97

Selection of soil contact models

In soil discrete element simulations, the JKR contact model accurately simulates the cohesive behavior between soil particles, particularly for wet or clayey soils (such as clay, saline-alkali soils, etc.) (*Tao et al.*, *2023*). This model is based on Hertz contact theory and simultaneously accounts for surface energy effects caused by moisture or viscous substances. It accurately characterizes elastic contact forces and surface adhesion forces between particles, reproduces the “contact-separation” hysteresis phenomenon, and equivalently simulates capillary forces. Therefore, the Hertz-Mindlin with JKR model was selected as the contact parameter for soil simulation.

Simulation parameters

The material parameters involved in this study include key mechanical properties such as the density, Poisson's ratio, and shear modulus of soil and steel. These parameters were determined through experimental measurements and supplemented with reference data from the literature(*Wang et al.*, *2024*). Specific values are presented in Table 3.

Table 3

Intrinsic parameters of soil and steel

Parameters	Soil	Metal
Density [kg/m³]	2655	7850
Poisson ratio	0.38	0.3
Shear modulus [Pa]	1.3×10^6	7.9×10^{10}

The contact parameters studied primarily include the soil surface energy in the JKR model, along with the collision recovery coefficient, static friction coefficient, and rolling friction coefficient between soil-soil and soil-steel interfaces. These parameters were obtained by combining the experimental measurement ranges in Table 3 with simulation calibration methods, with specific values shown in Table 4. The soil surface energy parameter for the JKR model referenced recommended values from the EDEM software GEMM database and other literature (*Jin et al.*, *2024*). Based on these fundamental parameter values, a soil particle model was constructed.

Experiments were designed for parameter calibration to examine the impact of parameter variations on soil stiffness during penetration tests. The discrete element soil penetration test simulation process (Figure 10) followed the actual penetration test procedure, with the cone penetrometer sinking at a constant speed of 20 mm/s (consistent with the actual test). To ensure simulation accuracy, the EDEM simulation applied a 40 mm displacement to the pressure plate. The force load on the cone penetration rod, representing soil firmness, was obtained through EDEM post-processing.

Table 4

Simulation contact parameter range

Parameters	Encoding	
	-1	1
Soil-Soil Collision Recovery Coefficient A	0.2	0.7
Soil - Soil Static Friction Coefficient B	0.3	0.8
Soil - Soil Rolling Friction Coefficient C	0.1	0.6
Soil-Steel Impact Recovery Coefficient D	0.05	0.55
Soil-Steel Static Friction Coefficient E	0.35	0.65
Soil-to-Steel Rolling Friction Coefficient F	0.05	0.25
JKR Model Soil Surface Energy G /[J·m⁻²]	4.6	17.6

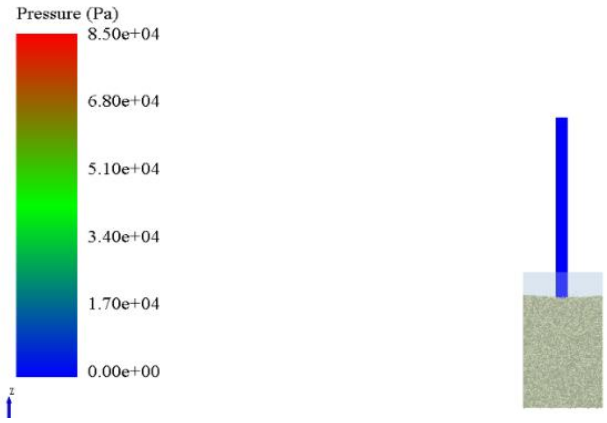

Fig. 10 - Soil Penetration Test

Plackett-Burman test

Soil penetration simulation tests (Figure 10) were employed for parameter optimization. Using the force exerted on the cone penetration rod as the evaluation metric, 12 Plackett-Burman experiments were designed using Design-Expert software to screen for significantly influential contact parameters. The experimental design included 7 parameters under investigation (A to G) and 4 dummy parameters (H to K), with each parameter set at two levels (high and low, coded as -1 and 1, respectively). To ensure data reliability, each test was repeated five times, and the final average value was taken as the soil firmness result for that test group.

Steepest climb test

After screening significant influencing parameters through Plackett-Burman experiments, the steepest ascent method was employed to optimize parameter ranges. Non-significant parameters were set to the midpoint of their measured ranges, while significant parameters were incremented stepwise according to preset increments. Soil firmness values obtained from each simulation experiment were recorded, and comparative analysis was conducted by calculating the relative error between simulation results and measured data (*Xiang et al.*, *2019*).

BOX-Behnken test

Based on the parameter combinations optimized using the steepest ascent method, further investigations were conducted to examine the influence patterns of different parameter configurations on soil firmness error values. Following experimental design methodology, each significant factor was assigned to low, medium, and high levels, resulting in 17 test groups, including 5 level-0 trials serving as baseline controls.

RESULTS

Table 5 presents the Plackett-Burman experimental design and its corresponding results, where A to G represent the parameter coding values. Analysis of variance conducted using Design-Expert software indicates the significance levels of each parameter's effect, as shown in Table 5.

Table 5

Design and results of Placket -Burman test

Serial Number	factor											Soil Firmness
	A	B	C	D	E	F	G	H	I	J	K	[kPa]
1	-1	1	1	-1	1	1	1	-1	-1	-1	1	88.85
2	-1	1	1	1	-1	-1	-1	1	-1	1	1	84.9
3	1	-1	1	1	-1	1	1	1	-1	-1	-1	86.31
4	-1	-1	-1	-1	-1	-1	-1	-1	-1	-1	-1	78.06
5	1	-1	1	1	1	-1	-1	-1	1	-1	1	83.9
6	1	1	-1	1	1	-1	-1	-1	-1	1	-1	101.03
7	1	1	-1	-1	-1	1	-1	1	1	-1	1	102.16
8	-1	-1	1	-1	1	1	-1	1	1	1	-1	72.5
9	-1	1	-1	1	1	-1	1	1	1	-1	-1	94.9
10	1	1	1	-1	-1	-1	1	-1	1	1	-1	107
11	-1	-1	-1	1	-1	1	1	-1	1	1	1	84.76
12	1	-1	-1	-1	1	-1	1	1	-1	1	1	95.9

Table 6

Parameter Significance Analysis Based on Soil Compaction

Source	Sum of Squares	df	Mean Square	F-value	p-value
model	1147.29	7	163.90	26.78	0.0033**
A	435.97	1	435.97	71.24	0.0011**
B	499.36	1	499.36	81.60	0.0008**
C	92.69	1	92.69	15.15	0.0177*
D	6.26	1	6.26	1.02	0.3689
E	3.11	1	3.11	0.5084	0.5152
F	6.83	1	6.83	1.12	0.3505
G	103.08	1	103.08	16.48	0.0148*
Residual	24.48	4	6.12		
Cor Total	1171.77	11			

*Note: ** indicates extremely significant（P＜0.01）; * indicates significant（P＜0.05）, The same applies below.*

According to the statistical analysis results in Table 6, the regression model is statistically significant ($p<0.05$). Specifically, the effects of independent variables A, B, C and G on soil firmness all reached a significant level<0.05). The significance ranking of each factor is as follows: B (Most significant impact)> A > G > C (least impact). The effects of the other examined factors on soil firmness did not reach statistical significance ($p>0.05$).

Table 7 presents the steepest slope test plan and results analysis. The findings indicate that as A, B and G increase, the simulated soil firmness gradually rises, while the relative error between simulation and measured results first decreases and then increases. Among these, Test 3 exhibits the smallest relative error in angle of repose, suggesting that the optimal parameter range lies near this test level. Therefore, subsequent Box-Behnken experiments centered on level 3 (level 0), with levels 2 and 4 serving as low (-1) and high (+1) levels, respectively. Specific parameter settings were: A = 0.3, 0.4, 0.5; B = 0.4, 0.5, 0.6; G = 7.2, 9.8, 12.4 J/m².

Table 7

Design and results of the steepest ascent test

Serial Number	factor			Soil Firmness [kPa]	Relative error [%]
	A	B	G [J/m²]		
1	0.2	0.3	4.6	76.6104	6.8%
2	0.3	0.4	7.2	77.8434	5.3%

Serial Number	factor			Soil Firmness [kPa]	Relative error [%]
	A	B	G [J/m²]		
3	0.4	0.5	9.8	78.8298	4.1%
4	0.5	0.6	12.4	78.64896	4.32%
5	0.6	0.7	15	71.83458	12.61%
6	0.7	0.8	17.6	68.4315	16.75%

Table 8 presents the Box-Behnken experimental design and results, where A, B, and G represent the coded values for soil static friction coefficient, soil collision rebound coefficient, and soil surface energy in the JKR model, respectively. Based on these experimental results, a second-order regression model for the three independent variables (coded values) of soil firmness error was established using Design-Expert software.

The regression model is as follows:

$$Y=2.960-0.4875A-0.6125B-0.5250G-0.5750AB+0.400AG+2.05BG+0.9075A^2+1.41B^2+2.08G^2 \quad (20)$$

Table 8

Design and results of the steepest ascent test

Serial Number	factor			Relative error *Y*
	A	B	G	[%]
1	-1	-1	0	2.6
2	1	-1	0	5.5
3	-1	1	0	3.9
4	1	1	0	5.8
5	-1	0	-1	9.8
6	1	0	-1	7.2
7	-1	0	1	3.7
8	1	0	1	2.3
9	0	-1	-1	4.7
10	0	1	-1	5.5
11	0	-1	1	7.5
12	0	1	1	5.2
13	0	0	0	2.7
14	0	0	0	4.1
15	0	0	0	5.9
16	0	0	0	5.6
17	0	0	0	3.5

Table 9 presents the results of the analysis of variance. The established quadratic polynomial regression model demonstrates extremely high significance ($P < 0.0001$). Both the coefficient of determination ($R^2 = 0.9943$) and the adjusted coefficient of determination ($R^2_{adj} = 0.9869$) approach 1, indicating that the regression model exhibits excellent fitting performance with high reliability and statistical significance.

Table 9

Box-Behnken test quadratic polynomial Model ANOVA

Source	Sum of Squares	df	Mean Square	F-value	p-value
model	59.00	9	6.56	24.68	0.0002**
A	1.90	1	1.90	7.16	0.0318*
B	3.00	1	3.00	11.30	0.0121*
G	2.21	1	2.21	8.30	0.0236*
AB	1.32	1	1.32	4.98	0.0609
AG	0.6400	1	0.6400	2.41	0.1646
BG	16.81	1	16.81	63.28	<0.0001**
A^2	3.47	1	3.47	13.05	0.0086**
B^2	8.34	1	8.34	31.40	0.0008**
G^2	18.26	1	18.26	68.74	<0.0001**
Residual	1.86	7	0.2656		
Lack of Fit	0.3875	3	0.1292	0.3510	0.7919
Pure Error	1.47	4	0.3680		
Cor Total	60.86	16			

Table 9 indicates that the quadratic terms A^2, B^2, and G^2 exert extremely significant effects on all evaluation indicators ($P < 0.01$). Single-factor effect analysis reveals that the linear terms A, B, and G significantly influence the evaluation indicators, with the magnitude of influence being B > G > A. In the interaction analysis, the BG interaction term exhibits a significant effect on the evaluation indicators, while the AB and AG interaction terms are insignificant ($P > 0.05$). This indicates a significant synergistic effect between the soil-soil static friction coefficient B and the soil surface energy G in the JKR model. The order of influence of interactions on the stiffness error value is: BG > AG > AB. As shown in Figure 11, the response surface analysis results for the interactions among the objective functions (soil firmness parameters) indicate that the error value of soil firmness increases with both the soil collision recovery coefficient and the JKR model soil surface energy. However, the error value does not exhibit a simple linear relationship with the increase of these two parameters. Instead, it follows a non-monotonic pattern of first decreasing and then increasing. The interaction between the two parameters means that the error value of soil firmness changes as both parameters increase simultaneously.

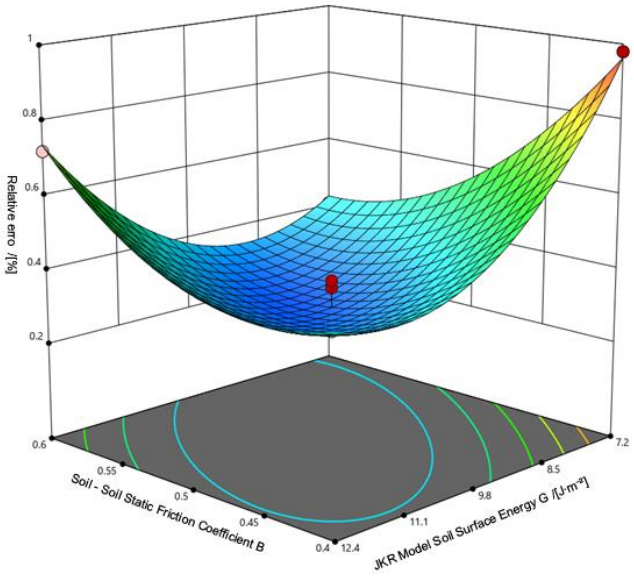

Fig. 11 - Interaction affecting firmness parameters

Parameter optimization and validation

Using the optimization module of Design-Expert software, parameter optimization was performed on the soil stiffness regression equation with a target value of 82.2 kPa based on measured soil stiffness. Through simulation verification of stiffness values from multiple sets of optimized solutions via penetration tests, the parameter set yielding the closest match between discrete element simulation results and experimental values was ultimately selected as the optimal solution.

The optimized solution obtained is as follows: Soil discrete element simulation parameters are set as: Soil-soil static friction coefficient 0.441, Soil-soil collision recovery coefficient 0.537, JKR contact model surface energy 9.551 J/m². Non-significant parameters adopted median experimental values: soil-soil rolling friction coefficient 0.15, soil-steel collision recovery coefficient 0.3, soil-steel static friction coefficient 0.5, soil-steel rolling friction coefficient 0.15.

The soil discrete element model was constructed in EDEM software using the optimized parameter settings. Through five repeated simulations of the soil penetration test, the obtained soil stiffness values were 78.5 kPa, 80.2 kPa, 79.8 kPa, 80.1 kPa and 80.0 kPa, with an average of 79.734 kPa. Compared to the measured results, the relative error was only 3.0%, indicating good consistency between the discrete element simulation results and the experimental data.

CONCLUSIONS

Based on the range of contact parameters, soil firmness was selected as the evaluation criterion, and Design-Expert software was used to design the Plackett-Burman experiment. Results indicate that the soil-soil static friction coefficient, soil-soil collision recovery coefficient, and surface energy of the JKR model exert the most significant influence on the soil firmness (rigidity at penetration).

The steepest climb test determined the optimal range for significant factors: soil-soil static friction coefficient 0.3–0.5, soil-soil collision recovery coefficient 0.4–0.6, and JKR model surface energy 7.2–12.4 J/m².

Box-Behnken test results indicated that the quadratic terms (A^2, B^2, G^2) of all three significant parameters (soil-soil static friction coefficient, soil-soil collision recovery coefficient, and JKR model surface energy) exerted extremely significant effects ($P<0.01$) on soil firmness. Additionally, a highly significant interaction existed between the interaction term BG (soil-soil static friction coefficient B and JKR model soil surface energy G) ($P<0.01$). The optimal parameter combination obtained through regression model optimization was: soil-soil static friction coefficient 0.441, soil-soil collision recovery coefficient 0.537, JKR contact model surface energy 9.551 J/m². Non-significant parameters were set to the median values from experimental data: soil-soil rolling friction coefficient 0.15, soil-steel collision recovery coefficient 0.3, soil-steel static friction coefficient 0.5, soil-steel rolling friction coefficient 0.15.

ACKNOWLEDGEMENT

This research was supported by the China Postdoctoral Science Foundation (2023M740866); the National Key Research and Development Program of China (2023YFD2001001); the Jiangsu Province Modern Agricultural Machinery Equipment and Technology Demonstration and Promotion Project of China (NJ2024-01); the Jiangxi Province Agricultural Machinery Equipment, Manufacturing, Popularization and Application Integration Pilot Project (YCTY202403-02-02).

REFERENCES

[1] Adajar, J. B., Alfaro, M., Chen, Y., Zeng, Z. (2021). Calibration of discrete element parameters of crop residues and their interfaces with soil, *Computers and Electronics in Agriculture*, Vol. 188, pp. 106349, London/England. DOI: https://doi.org/10.1016/j.compag.2021.106349

[2] Aikins, K. A., Ucgul, M., Barr, J. B, Jensen, T. A, Antille, D. L, & Desbiolles, J. M (2021). Determination of discrete element model parameters for a cohesive soil and validation through narrow point opener performance analysis, *Soil and Tillage Research*, Vol. 213, pp. 105–123, Netherlands. DOI: https://doi.org/10.1016/j.still.2021.105123

[3] Bahrami, M., Naderi-Boldaji, M., Ghanbarian, D., Ucgul, M., Keller, T. (2020). Simulation of plate sinkage in soil using discrete element modelling: Calibration of model parameters and experime ntal validation, *Soil and Tillage Research*, Vol. 203, pp.104700, Netherlands. DOI: https://doi.org/10.1016/j.still.2020.104700.

[4] Diao, H., Ye, W., Zhang, Z., Liu, X., Zhao, Z., Zeng, F., Li, X., Cui, J., Liu, Y. (2024). Measu rement of the physical parameters of peanut seeds and calibration of the discrete element para -meters, *INMATEH Agricultural Engineering*, Vol.72, no.1, pp.444–453, Bucharest/Romania. DOI: https://doi.org/10.35633/inmateh-72-39.

[5] He, X., Ma, S., Liu, Z., Wang, D., Shang, S., Li, G., Li, H. (2024). Calibration and testing of saline soil parameters based on EDEM discrete element methodology. *INMATEH Agricultural Engineering*, Vol.73, no.2, pp. 822–833, Bucharest/Romania. DOI: https://doi.org/10.35633/inmateh-73-69.

[6] Jin, F., Liu, D., Zhong, C., Yao, K., Tong, J., Jiang, Z. (2024). Parameter calibration and discrete element model of highland barley stem based on EDEM, *INMATEH Agricultural Engineering*, Vol.72, no.1, pp.363–374, Bucharest/Romania. DOI: https://doi.org/10.35633/inmateh-72-33.

[7] Liang X., Hu Z., Zheng L., et al. (2024). Optimization of the discrete element contact model for tidal flat soil and field shoveling experiment (滩涂土壤离散元接触模型优化与现场铲削试验). *Transactions of the Chinese Society of Agricultural Engineering (Transactions of the CSAE)*, vol.40, no.8, pp.107-115, Beijing/China. DOI:https:/doi.org/10.11975/j.issn.1002-6819.202401205

[8] Mi, J., Xie, H., Niu, P. (2025). Design and optimisation of rotary tiller blade for orchards in hilly mountainous areas based on the discrete element method. *INMATEH Agricultural Engineering*, Vol.76, no.2, pp. 177–186, Bucharest/Romania. DOI: https://doi.org/10.35633/inmateh-76-16.

[9] Pang J., Lin X., Chen S., Geng L., Zhou H., Jin X. (2023). Study on Measurement and Calibration Methods of Soil Parameters Used in Discrete Element Method (离散元法中所用土壤参数测量及标定方法研究). *Journal of Anhui Agricultural Sciences*, Vol. 51, no.18, pp. 6–11. Hefei/China. DOI: https://doi.org/10.3969/j.issn.0517-6611.2023.18.002

[10] Smith W., Peng H. (2013). Modeling of wheel-soil interaction over rough terrain using the discrete element method. *Journal of Terramechanics*, Vol.50, no.5-6, pp. 277–287, England. DOI: https://doi.org/10.1016/j.jterra.2013.09.002

[11] Sun J., Liu Q., Yang F., Liu Z., Wang Z. (2022). Calibration of Discrete Element Simulation Parameters of Sloping Soil on Loess Plateau and Its Interaction with Rotary Tillage Components (黄土高原坡地土壤与旋耕部件互作离散元仿真参数标定). Transactions of the Chinese Society for Agricultural Machinery, vol.53, no.1, pp. 63-73. Beijing/China. DOI: https://doi.org/10.6041/j.issn.1000-1298.2022.01.007

[12] Tao, C., Mo, Z., Lu, F., Li, Z., Su, D., Zhang, Y. (2023). Measurement of physical property parameters and simulative calibration of DEM parameters for green onion seeds. *INMATEH Agricultural Engineering*, Vol.70, no.2, pp.137–146, Bucharest/Romania. DOI: https://doi.org/10.35633/inmateh-70-13.

[13] Tian, L., Li, H., Zhang, X., Liu, C. (2024). Discrete element method simulation of rice grain stacking characteristics. *INMATEH Agricultural Engineering*, Vol.73, no.3, pp. 554–561, Bucharest/Romania. DOI: https://doi.org/10.35633/inmateh-74-49.

[14] Tian X., Cong X., Qi J., Guo H., Li M., Fan X. (2021). Parameter Calibration of Discrete Element Model for Corn Straw-Soil Mixture in Black Soil Areas(黑土区玉米秸秆-土壤混料离散元模型参数标定). *Transactions of the Chinese Society of Agricultural Engineering (Transactions of the CSAE)*, Vol. 52, no.10, pp. 100–108,242, Beijing/China.DOI:https://doi.org/10.6041/j.issn.1000-1298.2021.10.010

[15] Ucgul M., Fielke J. M., Aunders C. (2014). Three-dimensional discrete element modelling (DEM) of tillage: Accounting for soil cohesion and adhesion. *Biosystems Engineering*, Vol.129, pp. 298-306, USA. DOI: https://doi.org/10.1016/j.biosystemseng.2014.11.006

[16] Wang D., Lu T., Zhao Z., Shang S., Zheng S., Liu J. (2024). Calibration of Discrete Element Simulation Parameters for Cultivated Soil Layer in Coastal Saline Alkali Soil (滨海盐碱地耕作层土壤离散元仿真参数标定方法). *Transactions of the Chinese Society of Agricultural Engineering (Transactions of the CSAE)*, Vol.55, no.11, pp. 240–249, Beijing/China.
DOI:https:/doi.org/10.6041/j.issn.1000-1298.2024.11.025

[17] Xiang W., Wu M., Lü J., Quan W., Ma L., Liu J. (2019). Calibration of simulation physical parameters of clay loam based on soil accumulation test (基于堆积试验的黏壤土仿真物理参数标定). *Transactions of the Chinese Society of Agricultural Engineering*, vol.35, no.12, pp. 116–123, (in Chinese with English abstract), Beijing/China. DOI: https://doi.org/10.11975/j.issn.1002-6819.2019.12.014

[18] Zou Peishi, Ma Yongcai, Wang Hanyang, Mao Xin, Chen Peng. (2025). Calibration and testing of discrete element simulation parameters of albic soil in Sanjiang Plain (三江平原地区白浆土离散元仿真参数标定与试验). *Agricultural Research in the Arid Areas*, vol.43, no.05, pp.280-289+312, Yangling/China. DOI: https://doi.org/10.7606/j.issn.1000-7601.2025.05.28

[19] Zhou L. (2022). DEM-based modelling of maize seeds and the simulation analysis and experimental study of the seed-sowing (基于离散元法的玉米种子建模及播种过程的仿真分析与试验研究), PhD dissertation, Jilin University, Jilin/China.

[20] Zhang J., Chen W., Zhu J., Yuan D., Xia M., Ding Y. (2021). Research status and the prospect of energy-saving technology of rotary tiller (旋耕机节能技术研究现状及展望). *Journal of Chinese Agricultural Mechanization*, vol.42, no.7, pp.182–189, Nanjing/China. DOI: https://doi.org/10.13733/j.jcam.issn.2095-5553.2021.07.27